

# We are IntechOpen, the world's leading publisher of Open Access books Built by scientists, for scientists

6,900

Open access books available

186,000

International authors and editors

200M

Downloads

Our authors are among the

154

Countries delivered to

TOP 1%

most cited scientists

12.2%

Contributors from top 500 universities



WEB OF SCIENCE™

Selection of our books indexed in the Book Citation Index  
in Web of Science™ Core Collection (BKCI)

Interested in publishing with us?  
Contact [book.department@intechopen.com](mailto:book.department@intechopen.com)

Numbers displayed above are based on latest data collected.  
For more information visit [www.intechopen.com](http://www.intechopen.com)



# Optical Coherence Tomography for Non-Contact Evaluation of Fastener Flushness

*James H. Wang and Michael R. Wang*

## Abstract

Outside of the medical field, spectral domain optical coherence tomography (SD-OCT) is sparsely used. As such, we explored the possibility and practicality of using SD-OCT as a tool to evaluate fastener flushness and countersink surface profiles. A SD-OCT device was built with a handheld galvanometer scanner that weighed only 0.5 lb. Not only it does not require scan center alignment, but it is also capable of quickly producing measurements of fastener flushness, radius, slant angle, countersink edge radius, and surface angle. With the X-Y two-line scanning method, measurements take only 90 ms. The SD-OCT device used to obtain these measurements uses a lens with 60 mm focal length and a broadband light source of 840 nm center wavelength and 45 nm spectral bandwidth. With these components, the SD-OCT device is able to provide an axial depth resolution of 8.5  $\mu\text{m}$  and a lateral resolution of 19  $\mu\text{m}$ . The axial depth resolution can be improved by using a wider bandwidth light source. Furthermore, the device is able to produce 3D surface profiles of fasteners and countersinks using multi-line scans.

**Keywords:** optical coherence tomography, fastener flushness, countersink, optical imaging, 3D surface profile

## 1. Introduction

High-speed objects such as racecars, bullet trains, aircrafts, and space crafts are dependent on flush surfaces in order to reach the desired aerodynamic performance. As such, inspection techniques are especially important to ensure fastener flushness. Available technology used to inspect fastener flushness and countersink surface profiles include handheld calipers and its modified version [1], laser line scanners [2], and structured light [3]. The contact caliper inspection suffers from gauge contact positioning error, visual gauge angular alignment error, measurement readout error, and inability of producing an instant inspection report. It is also difficult to translate the measurement data into a 3D surface profile. The laser line scanner measurement is a faster technique for accessing the fastener flushness, but it suffers from limited measurement precision and 3D surface profiling ability. The structured light measurement, in particular the fastCHECK introduced by 8tree Inc., offers impressive 5  $\mu\text{m}$  axial measurement resolution and can check the flushness of multiple fasteners. However, it is not capable of 3D surface profiling inspection of fastener tilting angle, fastener radius, and countersink surface angle.

Optical coherence tomography (OCT) is a low-coherence interferometry technique [4]. With the capability of high axial resolution and fast lateral scan imaging, OCT has been used to perform cross-sectional imaging of biological tissues [5] as well as topographic evaluation of surface roughness [6]. OCT has also been used for fingerprint acquisition [7, 8], inspection of fiber coils [9], surface and coating evaluation [10], evaluation of metallic material fractures [11], and nondestructive metrology of layered polymeric material [12]. We report the use of the spectral domain OCT (SD-OCT) [13–16], a faster OCT, for fastener flushness and countersink surface profile evaluation.

## 2. SD-OCT configuration, scanning, and resolution

SD-OCT utilizes a Michelson interferometer configuration to examine the interference between two split broadband light beams [4, 14, 15]. **Figure 1** shows the fiber-optic-based SD-OCT configuration which employs a superluminescent diode (SLD) light source; a fiber isolator; a  $2 \times 2$  fiber coupler; a fiber-coupled OCT spectrometer; a reference arm with a collimation lens, a focusing lens, and a reflection mirror; and a measurement arm with a collimation lens, a mirror, galvanometer scanners, and a focusing lens. The SLD light is split by the fiber coupler to illuminate the reference mirror and the fastener as shown in **Figure 1**. The surface scattered light from the fastener and the reflected light from the reference arm mirror are combined by the  $2 \times 2$  fiber coupler to form spectral-dependent interference signals at the OCT spectrometer. The signals are acquired and processed by Fourier transform to extract the fastener surface depth ( $Z$ ) scattering information, which is the A-scan depth profile information. A lateral scan (B-scan) on  $X$  direction on the fastener will yield a fastener surface  $X$ - $Z$  profile in the scanned line direction. A multi-line scan (C-scan), which takes multiple  $X$  scan lines at different  $Y$  positions, can produce a 3D ( $X$ - $Y$ - $Z$ ) surface profile of the measurement sample. When the fastener is absent in **Figure 1**, the SD-OCT can be used to evaluate the 3D countersink surface profile for countersink production quality inspection.

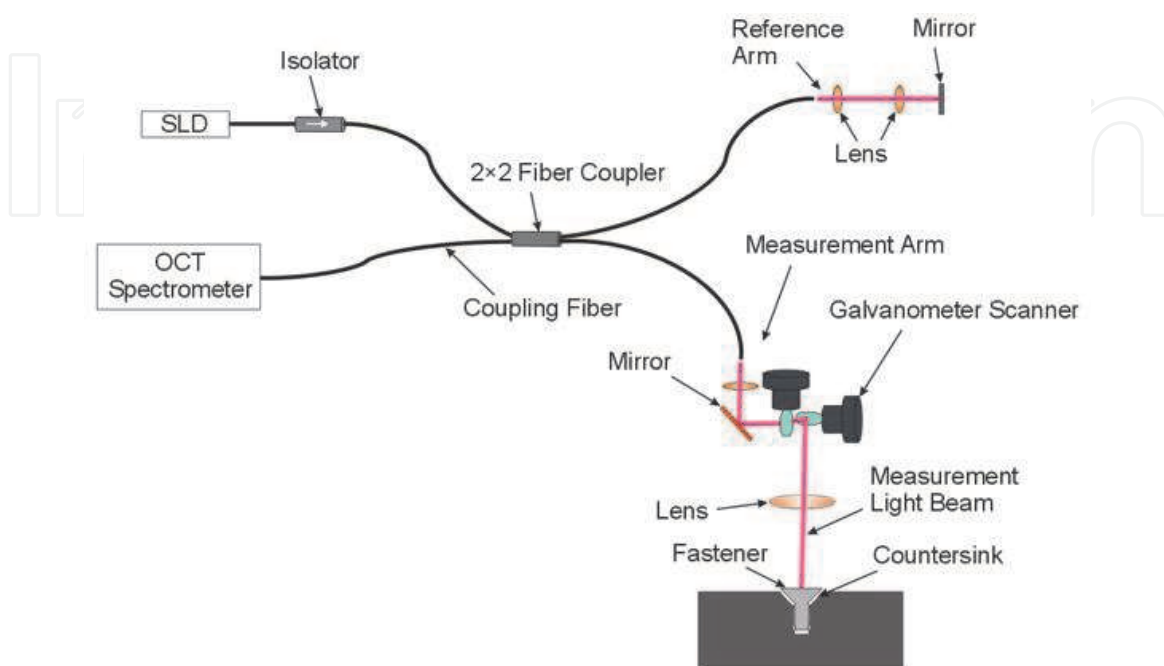


**Figure 1.**  
Schematic of SD-OCT system for fastener flushness evaluation.

We constructed a SD-OCT with a handheld scanner of only 0.5 lb. in weight as shown in **Figure 2** to facilitate easier fastener flushness evaluation. The schematic of the interior of the handheld scanner is also shown. The circular ring will have soft contact (using a mounted plastic or rubber ring) with the surrounding surface to help the user stabilize and align the scanner properly. As to be discussed in the following sections, the scanner circular ring does not need to be centered with the fastener or countersink. An X and Y two-axis scan would automatically determine the fastener or countersink center and evaluate the fastener slant angle or countersink surface angle.

The SD-OCT system (BIOptoscan OS-184, New Span Opto-Technology) is constructed in-house. An SLD (IPSSD0808, InPhenix) light source is used which has a center wavelength of 840 nm and a full width at half maximum spectral bandwidth of 45 nm. The selection of this light source is due to its availability in-house. For fastener flushness evaluation, it would be desirable in principle to select shorter SLD center wavelength yet with reasonable wide spectral bandwidth to attain a better axial resolution [17]. However, the choice of SLD (e.g., InPhenix) is quite limited. The OCT spectrometer using a line scan camera with 2048 pixels supports an axial depth measurement range of 3.65 mm in the air. The two-axis handheld galvanometer scanner in **Figure 2** is connected to the SD-OCT main unit through a control cable with a single-mode optical fiber. A data acquisition card (PCI-6251, National Instruments) and a camera link card (PCIe-1427, National Instruments) are used. The SD-OCT is operating at a line scan rate of 28 kHz. The Fourier transform data processing is performed by a computer. The handheld scanner's circular ring has a diameter of 3.6 cm, and the focusing lens has a focal length of 60 mm, which produces a focused beam spot size of 19  $\mu\text{m}$  on the sample.

For fast scan measurement, the line scan uses 512 measurement spot positions with 19  $\mu\text{m}$  scan spot center-to-center separation, producing no gap between adjacent spots. The field of view (FOV) is 9.73 mm which is enough for most fastener evaluation. When larger fasteners need to be evaluated, more measurement spots or some spot spacing can be included with a change in the programming of the scanner control voltage matrix. For the present line scan of 512 spots, it takes 22 ms. An X-Y perpendicular two-line scan takes 44 or 90 ms if including OCT image processing. This speed is fast enough for handheld fastener scan measurement without the concern of hand instability provided that the handheld scanner is resting on the measurement surface with a soft plastic or rubber ring spacer. If we need to perform multi-line C-scan of 128 lines of 128 spots per line, it takes 2.2 seconds. A  $256 \times 256$

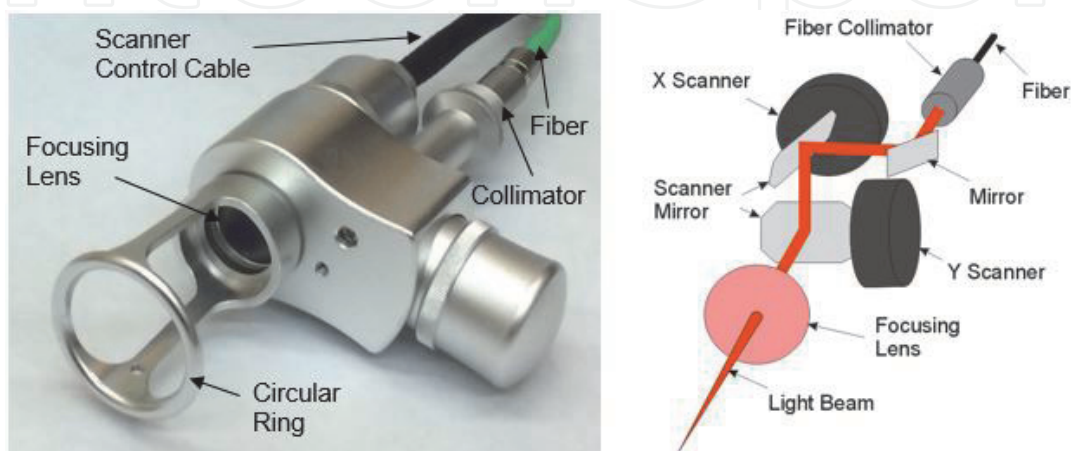


**Figure 2.**  
*Picture and schematic of the SD-OCT handheld scanner.*

C-scan takes about 7.6 seconds. This speed, which includes the OCT image processing time, is also reasonably fast.

The axial measurement resolution is set by the spectral bandwidth of the SLD light source. Due to the non-Gaussian spectral distribution of the SLD light source, the present axial resolution is determined to be 8.5  $\mu\text{m}$  in the air, which is better than most laser light scan measurements [2]. If using a 100 nm bandwidth light source, the SD-OCT axial resolution could be improved to 4.3  $\mu\text{m}$  in the air. The axial resolution can be further improved to  $\sim 3$   $\mu\text{m}$  by using a 150 nm bandwidth light source instead. The lateral resolution is currently set by the focused beam spot size to be 19  $\mu\text{m}$ , which is enough for fastener flushness evaluation. The lateral resolution may be improved by using shorter focal length lens on the scanner with the trade-off of a smaller FOV or by using a super-resolution technique with the trade-off of a longer scanning and image processing time [17].

### 3. Evaluation of fastener flushness

To perform fast fastener flushness evaluation using the SD-OCT without demanding center alignment of the scanner and fastener, we developed an  $X$ - $Y$  perpendicular two-line scan pattern to determine the fastener's center position, radius, relative tilting angle, and flushness with the surrounding surface. As schematically illustrated in **Figure 3**, the red  $X$ - $Y$  scan line is off-center. With the determination of fastener edge coordinate information  $(x_1, 0, h_{x1})$ ,  $(x_2, 0, h_{x2})$ ,  $(0, y_1, h_{y1})$ , and  $(0, y_2, h_{y2})$ , where height  $h$  is in respect to surrounding surface, we can determine the fastener surface center and height as.

$$(x_{center}, y_{center}, h_{center}) = \left( \frac{x_1 + x_2}{2}, \frac{y_1 + y_2}{2}, \frac{h_{x1} + h_{x2}}{2} + \frac{(h_{y2} - h_{y1})(y_1 + y_2)}{2(y_2 - y_1)} \right) \quad (1)$$

The height of the fastener surface center position is calculated under the assumption that the fastener head is a flat circle. Hence, the height does not account for the cavity. Using the center position calculated above, the radius of the fastener can also be determined as

$$R = \sqrt{\left(\frac{x_2 - x_1}{2}\right)^2 + y_{center}^2 + (h_{center} - h_{x1})^2} \quad (2)$$

By using the four edge coordinates established earlier, two vectors can be generated for the two scan lines. With these two vectors, taking the cross product will result in the normal vector,  $\hat{N}$ . Taking the dot product of this vector  $\hat{N}$  with the normal vector of the surrounding surface  $\hat{Z}$  will result in the tilting angle  $\theta$  of the fastener. Since the scans conducted with the handheld scanner utilize the circular ring, it is assumed that the surrounding surface is flat. Thus, the tilting angle  $\theta$  can be calculated as

$$\theta = \cos^{-1} \left( \frac{(x_2 - x_1)(y_2 - y_1)}{\sqrt{(y_2 - y_1)^2 (h_{x2} - h_{x1})^2 + (x_2 - x_1)^2 (h_{y2} - h_{y1})^2 + (x_2 - x_1)^2 (y_2 - y_1)^2}} \right) \quad (3)$$

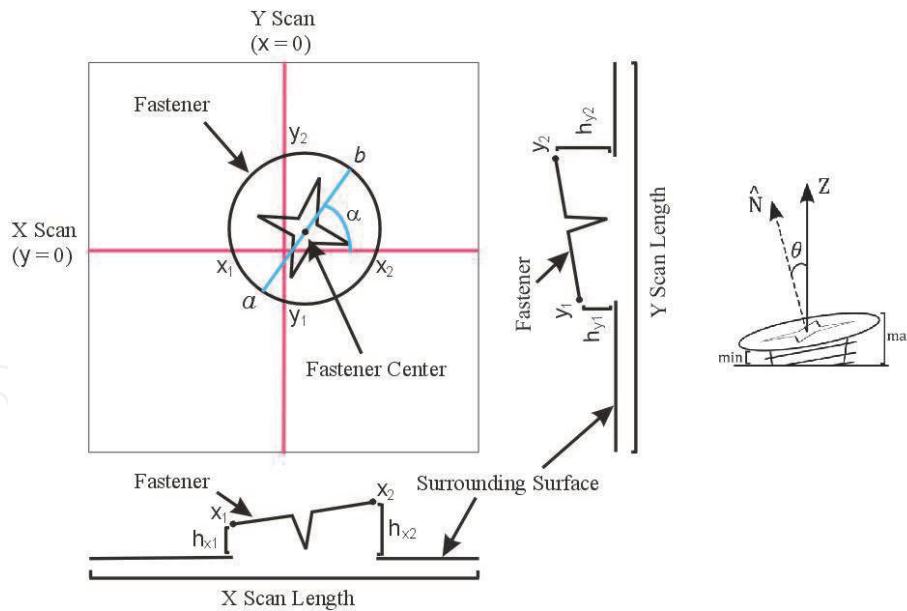


**Figure 3.**  
 Schematic for the measurement of fasteners.

To determine the flushness of the fastener, we can find the minimum and maximum heights  $h_a$  and  $h_b$  as shown in **Figure 3**. To do so, we first find the blue line slant angle  $\alpha$  as

$$\alpha = \tan^{-1} \left( \frac{(x_2 - x_1)(h_{y2} - h_{y1})}{(y_2 - y_1)(h_{x2} - h_{x1})} \right) \quad (4)$$

By using angle  $\alpha$ , new edge coordinates  $(x_a, y_a)$  and  $(x_b, y_b)$  can be determined:

$$(x_a, y_a) = (x_{center} - R \cos(\theta) \cos(\alpha), y_{center} - R \cos(\theta) \sin(\alpha)) \quad (5)$$

$$(x_b, y_b) = (x_{center} + R \cos(\theta) \cos(\alpha), y_{center} + R \cos(\theta) \sin(\alpha)) \quad (6)$$

Knowing these two points  $a$  and  $b$ , the minimum and maximum heights of the fastener with the surrounding surface can be calculated. The equations to calculate the height for both points are

$$h_a = h_{x1} + \frac{h_{x2} - h_{x1}}{x_2 - x_1} x_a + \frac{h_{y2} - h_{y1}}{y_2 - y_1} y_a \quad \text{and} \quad h_b = h_{x1} + \frac{h_{x2} - h_{x1}}{x_2 - x_1} x_b + \frac{h_{y2} - h_{y1}}{y_2 - y_1} y_b \quad (7)$$

To demonstrate the effectiveness of the fastener flushness evaluation, we acquired SD-OCT X-Y scan images of a fastener as shown in **Figure 4**. To minimize image line saturation and formation of image echo, the light source power and thus the image brightness are reduced. Based on the off-center information of the images, we obtained the coordinates  $x_1, x_2, y_1,$  and  $y_2$  and flushnesses  $h_{x1}, h_{x2}, h_{y1},$  and  $h_{y2}$ . Using the measurement technique mentioned above, we obtained the fastener radius of 3.53 mm which is close to the actual radius of 3.54 mm. The measured minimum and maximum flushness were 244.4 and 549.3  $\mu\text{m}$ , respectively. The determined tilting angle  $\theta$  and  $\alpha$  were  $2.47^\circ$  and  $-19.45^\circ$ , respectively. **Figure 5** shows a C-scan 3D image of the same fastener [18] acquired by  $256 \times 256$  scan matrix showing the capability of the SD-OCT system. The saved and

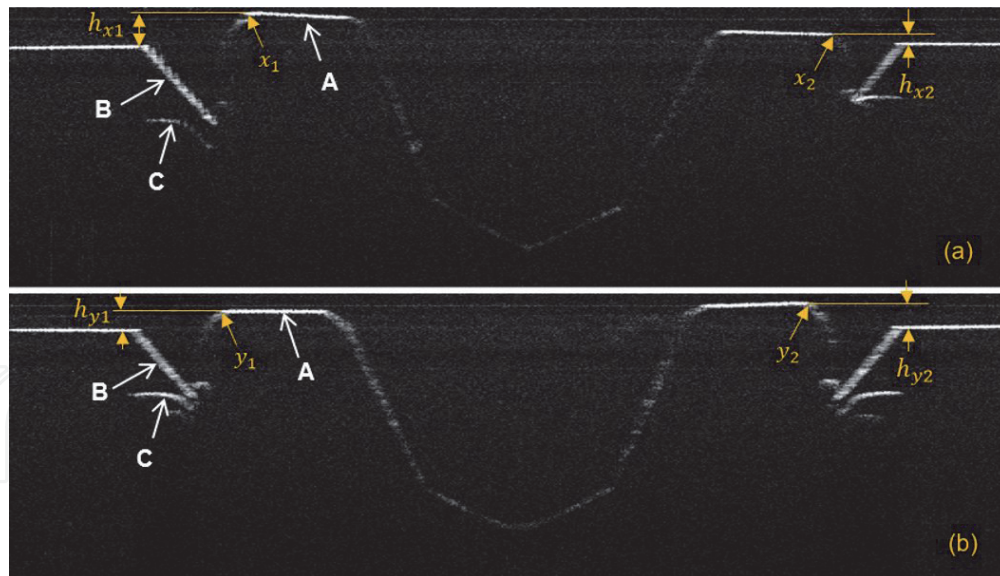


**Figure 4.** OCT X-Y scan image of a fastener with scanner center not aligned to the fastener center. (a) Image of X scan and (b) image of Y scan. The lateral scan range is 12 mm and the scan depth is 3.65 mm in the air. A is the fastener, B is the countersink, and C is the reflection image of the fastener edge by the countersink.

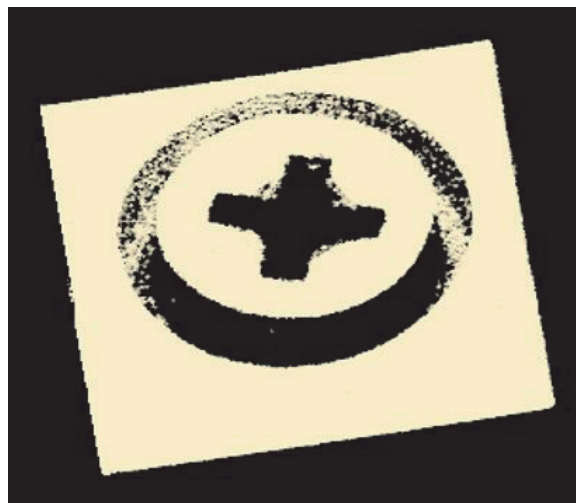


**Figure 5.** 3D OCT image of the fastener [18].

documented 3D image data can be extracted to obtain any portion of the B-scan image for inspection reporting.

#### 4. Evaluation of countersink surface profile

The seating of the fastener would depend on the quality of the countersink and underlying structure. For a cone shape countersink, it is important to evaluate its slant surface angle  $\beta$  as shown in **Figure 6**. To do so, we performed X-Y perpendicular two-line scan with scan center to be on any part of the cone shape slant surface without scanning through the countersink center screw hole. This can be ensured by not seeing a deep hole in the two line scan images. Instead, we should observe a curved scan surface line in each X and Y line scan image as illustrated in **Figure 6**. By taking the derivative on the X and Y scan data at the scan center O, we obtain

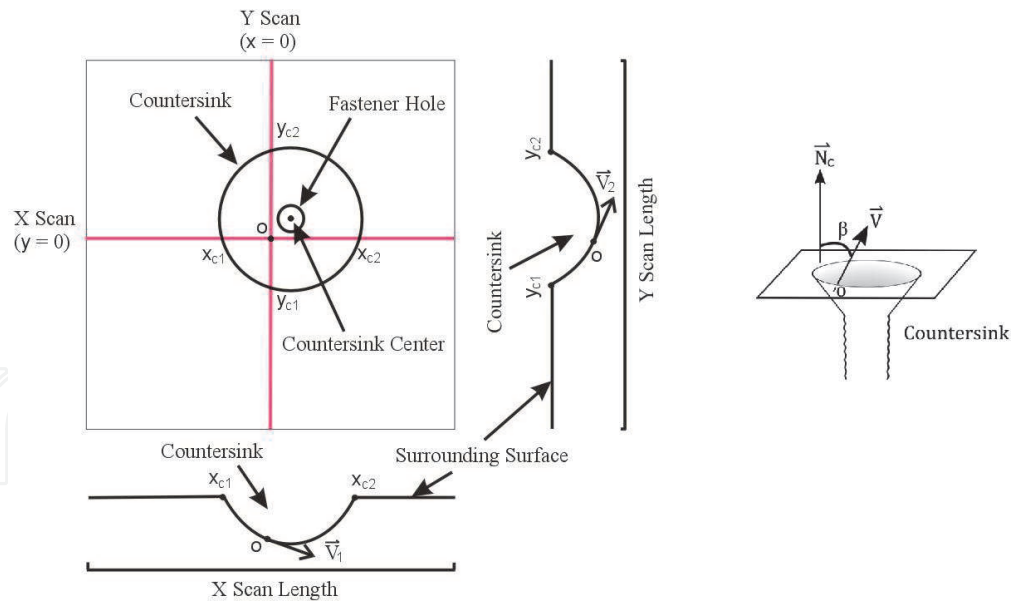


**Figure 6.**  
 Schematic of X-Y line scan measurement of a countersink.

two slopes and thus two tangential vectors  $\vec{V}_1$  and  $\vec{V}_2$ . The cross product of the two vectors gives us the countersink slant surface normal vector  $\vec{V}$ .

This surface normal vector  $\vec{V}$  is obtained from the X and Y scan data which is in reference to the handheld scanner's circular ring surface. This surface may be not exactly the same as the countersink outside surface. To determine the outside flat surface normal  $\vec{N}_c$  for slant surface angle  $\beta$  determination, we first determine the countersink edge coordinates  $(x_{c1}, 0, z_{xc1})$ ,  $(x_{c2}, 0, z_{xc2})$ ,  $(0, y_{c1}, z_{yc1})$ , and  $(0, y_{c2}, z_{yc2})$ . Then the surface normal vector  $\vec{N}_c$  is obtained.

$$\vec{N}_c = \langle (y_{c2} - y_{c1})(z_{xc1} - z_{xc2}), (x_{c2} - x_{c1})(z_{yc1} - z_{yc2}), (x_{c2} - x_{c1})(y_{c2} - y_{c1}) \rangle \quad (8)$$

Using this vector and the previously found surface normal vector, the slant angle of the countersink surface can be calculated by

$$\beta = \cos^{-1} \left( \frac{\vec{V} \cdot \vec{N}_c}{|\vec{V}| |\vec{N}_c|} \right) \quad (9)$$

Similar to the equation used to calculate the radius of the fastener head, the countersink radius can be calculated as

$$R_c = \sqrt{\left( \frac{x_{c2} - x_{c1}}{2} \right)^2 + \left( \frac{y_{c2} + y_{c1}}{2} \right)^2 + \left( \frac{z_{xc1} + z_{xc2}}{2} + \frac{(z_{yc2} - z_{yc1})(y_{c1} + y_{c2})}{2(y_{c2} - y_{c1})} - z_{xc1} \right)^2} \quad (10)$$

To demonstrate the effectiveness of countersink surface profile evaluation, we acquired SD-OCT X-Y scan images of a countersink as shown in **Figure 7**. The countersink slant surface angle  $\beta$  and radius  $R_c$  were found to be  $50.9^\circ$  and 4.59 mm

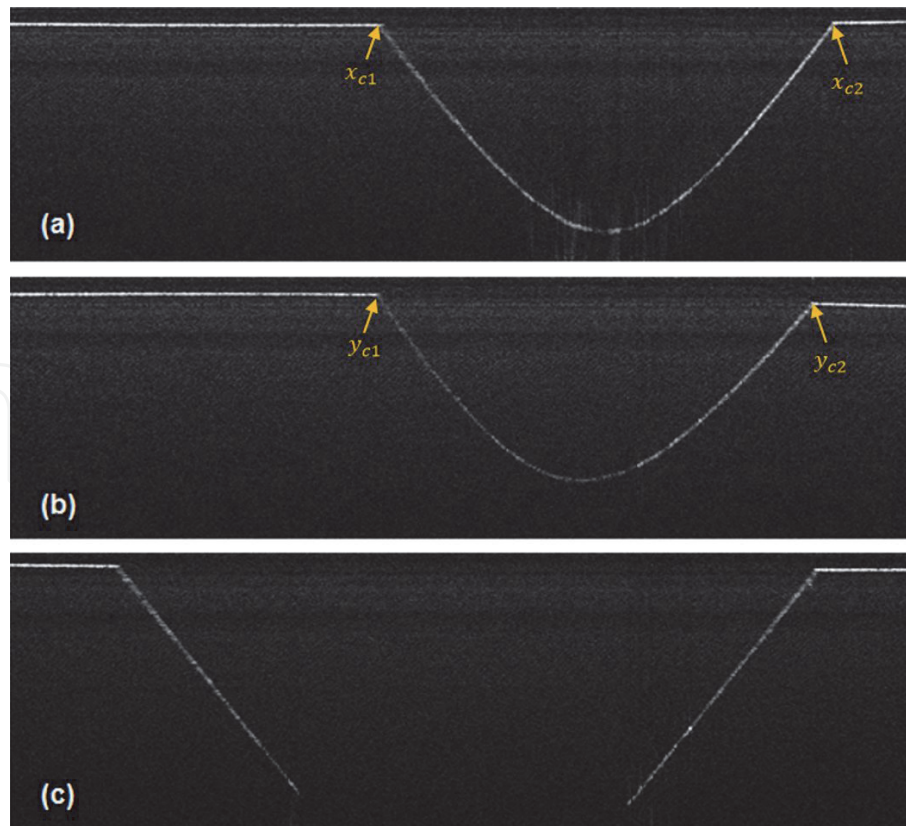


**Figure 7.** OCT X-Y scan image of a countersink with scanner center on any part of a countersink slant surface. (a) Image of X scan and (b) image of Y scan with lateral scan range of 16 mm and scan depth of 3.65 mm in the air. The countersink edge coordinates are  $x_{c1}$ ,  $x_{c2}$ ,  $y_{c1}$ , and  $y_{c2}$ . (c) Through center scan image of the countersink with lateral scan range of 12 mm.

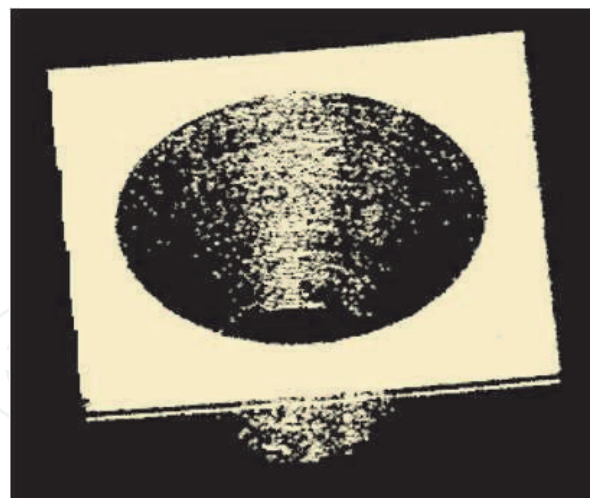


**Figure 8.** 3D OCT image of the countersink [18].

close to the actual value of  $50.5^\circ$  and 4.57 mm, respectively. **Figure 8** shows a C-scan 3D image of the same countersink [18] acquired by a  $256 \times 256$  scan matrix.

## 5. Conclusion

Considering that high-speed vehicles and aircraft demand high-quality inspection of fastener flushness and countersinks, the SD-OCT scanner would be a valuable inspection device. Using an X-Y scanning pattern with vector calculation not

only avoids center alignment of the scanner and fastener but also allows for quick evaluation of the fastener's radius, tilt angle, and flushness. Similarly, countersink evaluation also uses the *X-Y* scanning pattern to determine the countersink's radius and surface angle. In addition, the SD-OCT device is capable of producing 3D surface profiles by using multi-line C-scans. With all of these features, its high axial resolution on top of all these measurements show that this device has potential for practical use in fastener flushness and countersink evaluation.

### **Conflict of interest**

The authors declare no conflict of interest.

### **Author details**

James H. Wang<sup>1</sup> and Michael R. Wang<sup>2\*</sup>

<sup>1</sup> New Span Opto-Technology Inc., Miami, FL, USA

<sup>2</sup> Department of Electrical and Computer Engineering, University of Miami, Coral Gables, FL, USA

\*Address all correspondence to: [mwang@miami.edu](mailto:mwang@miami.edu)

### **IntechOpen**

© 2020 The Author(s). Licensee IntechOpen. Distributed under the terms of the Creative Commons Attribution - NonCommercial 4.0 License (<https://creativecommons.org/licenses/by-nc/4.0/>), which permits use, distribution and reproduction for non-commercial purposes, provided the original is properly cited. 

## References

- [1] Alberts DG. Countersink Depth Gauge. Patent US5758433; 1998
- [2] Zhang H, Tao W, Liu M, Zhao H. A laser scanning system for the inspection of fasteners in railways. *Lasers in Engineering*. 2013;24:229
- [3] Ren SW, Liu WW, Liu H, Liu MH, Liu WH, Yang JF, et al. Tao, Structured light-based high-speed detection system and method for railway fastener, patent CN102221553A; 2011
- [4] Huang D, Swanson EA, Lin CP, Schuman JS, Stinson WG, Chang W, et al. Optical coherence tomography. *Science*. 1991;254:1178-1181. DOI: 10.1126/science.1957169
- [5] Izatt JA, Hee MR, Swanson EA, Lin CP, Huang D, Schuman JS, et al. Micrometer-scale resolution imaging of the anterior eye in vivo with optical coherence tomography. *Archives of Ophthalmology*. 1994;112:1584. DOI: 10.1001/archophth.1994.01090240090031
- [6] Amaral MM, Ruele MP, Caly JP, Samad RE, Vieira ND, Freitas AZ. Roughness measurement methodology according to DIN 4768 using optical coherence tomography (OCT). *Proceedings of SPIE*. 2009;7390:73900Z. DOI: 10.1117/12.827748
- [7] Darlow LN, Akhoury SS, Connan J. A review of state-of-the-art speckle reduction techniques for optical coherence tomography fingertip scans. *Proceedings of SPIE*. 2015;9445:944523. DOI: 10.1117/12.2180537
- [8] Akhoury SS, Darlow LN. Extracting subsurface fingerprints using optical coherence tomography. *IEEE Xplore*. 2015:184
- [9] Li Z, Meng Z, Wang L, Liu T, Yao SX. Tomographic inspection of fiber coils using optical coherence tomography. *IEEE Photonics Technology Letters*. 2015;27:549. DOI: 10.1109/LPT.2014.2384837
- [10] Cerrotta S, Morel EN, Torga JR. Scanning optical coherence tomography applied to the characterization of surfaces and coatings. *Procedia Materials Science*. 2015;9:142. DOI: 10.1016/j.mspro.2015.04.018
- [11] Hutiu G, Duma VF, Demian D, Bradu A, Podoleanu AG. Surface imaging of metallic fractures using optical coherence tomography. *Applied Optics*. 2014;53:5912. DOI: 10.1364/AO.53.005912
- [12] Meemon P, Yao J, Lee K-S, Thompson KP, Ponting M, Baer E, et al. Optical coherence tomography enabling nondestructive metrology of layered polymeric GRIN material. *Scientific Reports*. 2013;3:1709. DOI: 10.1038/srep01709
- [13] Kim JS, Ishikawa H, Gabriele ML, Wollstein G, Bilonick RA, Kagemann L, et al. Retinal nerve fiber layer thickness measurement comparability between time domain optical coherence tomography (OCT) and spectral domain OCT. *IVOS*. 2010;51:896. DOI: 10.1167/iavs.09-4110
- [14] de Boer JF, Cense F, Hyle Park B, Pierce MC, Tearney GJ, Bouma BE. Improved signal-to-noise ratio in spectral-domain compared with time-domain optical coherence tomography. *Optics Letters*. 2003;28:2067. DOI: 10.1364/OL.28.002067
- [15] Wojtkowski M. High-speed optical coherence tomography: Basics and applications. *Applied Optics*. 2010;49:D30. DOI: 10.1364/AO.49.000D30
- [16] Drexler W, Liu M, Kumar A, Kamali T, Unterhuber A, Leitgeb RA.

Optical coherence tomography today:  
Speed, contrast, and multimodality.  
Journal of Biomedical Optics. 2014;**19**:  
071412. DOI: 10.1117/1.JBO.19.7.071412

[17] Shen K, Liu H, Baig S, Wang MR.  
Improving lateral resolution and image  
quality of optical coherence tomography  
by the multi-frame superresolution  
technique for 3D tissue imaging.  
Biomedical Optics Express. 2017;**8**:4887.  
DOI: 10.1364/BOE.8.004887

[18] Wang JH, Wang MR. Handheld  
non-contact evaluation of fastener  
flushness and countersink surface  
profiles using optical coherence  
tomography. Optics Communications.  
2016;**371**:206. DOI: 10.1016/j.optcom.  
2016.03.069